Temporal variations in sea ice resistivity: Resolving anisotropic microstructure through cross-borehole DC resistivity tomography

K. A. Jones,[1] M. Ingham,[1] D. J. Pringle,[2,3] and H. Eicken[2]

Received 10 December 2009; revised 10 August 2010; accepted 25 August 2010; published 24 November 2010.

[1] The distribution and connectivity of brine pockets in first year sea ice has a determining influence on the bulk properties of the ice and its interaction with the environment. The structure of the brine network depends upon both temperature and salinity, and a full understanding of the temporal evolution of sea ice physical properties requires measurements that are sensitive to the microstructure and can also be made without disturbing the natural state of the ice. Direct current resistivity techniques are suited to this as the brine fraction is orders of magnitude more conductive than solid ice. However, due to the preferential vertical alignment of brine inclusions, the bulk resistivity of first year sea ice is anisotropic. Although this makes the interpretation of surface resistivity soundings extremely difficult, consideration of the theory of resistivity measurements in an anisotropic medium shows that the anisotropic resistivity structure may be resolved through cross-borehole measurements. Borehole pairs with one current and one potential electrode in each hole allow the determination of the horizontal component of the anisotropic bulk resistivity (ρ_H). Use of four boreholes allows an estimate of the geometric mean resistivity (ρ_m) to be derived. Combining these measurements allows calculation of the vertical resistivity (ρ_V). This is illustrated by measurements made in first year sea ice near Barrow, Alaska in April–June 2008. Over this period significant changes in resistivity are observed which may be shown to be related to both the brine volume fraction and the microstructure of the ice.

Citation: Jones, K. A., M. Ingham, D. J. Pringle, and H. Eicken (2010), Temporal variations in sea ice resistivity: Resolving anisotropic microstructure through cross-borehole DC resistivity tomography, *J. Geophys. Res.*, *115*, C11023, doi:10.1029/2009JC006049.

1. Introduction

[2] Sea ice covers a large area of high-latitude ocean in the Arctic and Antarctic regions. While sea ice extent varies seasonally, at maximum approximately 7% of the Earth's surface is covered, making sea ice one of the largest biomes on Earth. Not only does sea ice regulate the exchange of heat between the ocean and the atmosphere, but its permeability to fluids controls brine exchange with the ocean, and its physical strength allows it to provide a surface for ice based activities. Despite the importance of sea ice, a detailed understanding and representation of many of its physical properties is still lacking. This is needed to give greater accuracy to both climate models and global circulation models [*Dieckmann and Hellmer*, 2003]. In this paper we present a significant advance toward a better understanding of the physical properties of sea ice and their seasonal evolution with temperature, salinity and brine volume fraction.

[3] During the formation of sea ice, brine becomes trapped in pockets within the solid ice matrix. These range in size from submillimeter pores to large connected networks of channels several millimeters in diameter and extending over several decimeters. The connectivity of the brine pockets is highly sensitive to variations in temperature and bulk ice salinity, and strongly affects physical, optical [*Eicken*, 2003], and biological properties [*Krembs et al.*, 2000] of sea ice. It is through these properties that sea ice has an influence on the global climate [*Comiso*, 2003] and ecosystems. An understanding of the manner in which the internal microstructure of sea ice changes in response to changes in temperature and salinity is therefore crucial for a fuller understanding of the role that sea ice plays in a range of contexts. The existence and connectivity of brine channels in the ice affects the transport of heat through the ice [*Perovich*, 1998; *Weeks*, 1998]. By estimating the latent heat release associated with convective overturning and refreezing of brine, *Pringle et al.* [2007] have estimated that internal brine motion within the ice may somewhat enhance the overall heat flux. Brine inclusions also control the manner in which the ice interacts with electromagnetic radiation [*Hallikainen and Winebrenner*,

[1]School of Chemical and Physical Sciences, Victoria University of Wellington, Wellington, New Zealand.
[2]Geophysical Institute, University of Alaska Fairbanks, Fairbanks, Alaska, USA.
[3]Arctic Region Supercomputing Centre, University of Alaska Fairbanks, Fairbanks, Alaska, USA.

0148-0227/10/2009JC006049

1992; *Cherkaeva and Golden*, 1998], while fluid permeability is important for nutrient transport through the ice [*Fritsen et al.*, 1994]. Theoretical calculations of the physical properties of sea ice have generally been based on effective medium theories [e.g., *Tinga et al.*, 1973] and, more recently, on percolation theory [*Golden et al.*, 1998, 2007]. Nevertheless, despite the relevance of the microstructure of sea ice to determining its role in the global climate system, there are few field measurements of the temporal variation in the physical properties of sea ice with which such theoretical calculations can be compared.

[4] The internal structure of sea ice ought to be able to be studied using any transport property to which the brine and ice components contribute differently. The microstructure, thermal evolution, fluid transport and permeability of sea ice brine inclusions have been studied by several authors using NMR techniques [*Callaghan et al.*, 1998, 1999; *Eicken et al.*, 2000; *Mercier et al.*, 2005], bail test and fluorescent tracer methods [*Freitag and Eicken*, 2003], X-ray computed tomography [*Kawamura*, 1988; *Pringle et al.*, 2009b], and impedance measurements [*Notz and Worster*, 2008; *Pringle et al.*, 2009a]. However, in practice there are severe difficulties in making accurate measurements as most such methods inevitably disturb the ice from its natural state, such as brine loss from samples that need to be extracted for measurements in the laboratory or artificial brine motion induced by insertion of large probes.

[5] In this context, measurements of electrical resistivity hold some promise, since the large resistivity contrast between brine and solid ice opens a path toward indirect probing of other key ice properties. Furthermore, direct current (DC) geoelectric soundings, widely used in shallow geophysical studies, are generally made using surface electrodes and do not therefore disturb the natural structure of the subsurface. However, due to the preferential vertical alignment of brine inclusions, the bulk resistivity of sea ice is anisotropic and, as a result, surface resistivity soundings can be shown [e.g., *Bhattacharya and Patra*, 1968] to be sensitive to only the geometric mean resistivity of the anisotropic medium. This has been clearly noted in previous resistivity measurements made on sea ice [e.g., *Fujino and Suzuki*, 1963; *Thyssen et al.*, 1974; *Timco*, 1979; *Buckley et al.*, 1986; *Ingham et al.*, 2008] which have also shown that surface soundings underestimate the true thickness of the anisotropic sea ice cover. This makes the interpretation of soundings in terms of variation of geometric mean resistivity with depth problematic.

[6] Recently *Ingham et al.* [2008] have demonstrated that an alternative DC resistivity technique, that of cross-borehole tomography, can be used to measure the horizontal component of the anisotropic resistivity structure of sea ice. This technique involves making resistivity measurements using vertical strings of electrodes frozen into the ice while it is relatively thin and that are subsequently embedded into the growing ice sheet. Although insertion of electrode strings, and their subsequent freezing in, disturbs the ice structure immediately adjacent to the boreholes, the bulk of ice between the electrode strings is undisturbed and it is through this that current passes. Such measurements therefore largely sample ice in its natural state. *Ingham et al.* [2008] reported trial measurements made at Barrow, Alaska that clearly suggested that changes in the horizontal component of resistivity of the ice occurred over the period of spring warming.

[7] In this paper we discuss, and present results from, a further development of the use of resistivity techniques to study the physical properties of sea ice. We start by readdressing, from the point of view of the theory of resistivity measurements in an anisotropic medium, the ability or inability of cross-borehole techniques to measure not only the horizontal component of the anisotropic resistivity, but also the vertical component and the geometric mean resistivity. Following consideration of an infinite anisotropic medium (section 2) we consider an anisotropic medium bounded by air above and by a highly conducting half-space, representative of seawater, below (section 3). We demonstrate how in this situation, in addition to resolving the horizontal component of resistivity, cross-borehole measurements supported by the results of model calculations can yield the geometric mean resistivity and its variation with depth in the ice. This consequently allows the derivation of the vertical component of the resistivity, thus determining the complete resistivity structure. We illustrate this both with inversions of synthetic data generated from forward numerical calculations, and by presenting results from the actual application to real sea ice (section 4). These results, from a series of 6 sets of measurements made near Barrow Alaska over the period of spring warming, clearly show a temporal evolution in the electrical properties of sea ice. They indicate that the resistivity technique holds much promise as a vehicle for developing a greater understanding of the temporal variation of the microstructure of sea ice and the impact of this on the physical properties of sea ice that are crucial to its role in the climate system.

2. Electrical Resistivity Measurements in an Infinite Uniform Anisotropic Medium

[8] In first year sea ice formed under quiescent conditions the preferential vertical alignment of the brine inclusions means that the bulk resistivity structure of the ice is anisotropic, with the vertical component of the bulk resistivity lower than the horizontal component. Although it is possible that in the presence of steady ocean currents the horizontal resistivity itself may exhibit some anisotropy, particularly in the case of landfast sea ice [*Kovacs and Morey*, 1978], in the present analysis we treat this as typically insignificant compared to the anisotropy between the vertical and horizontal resistivity.

[9] Following *Bhattacharya and Patra* [1968], as detailed in the Appendix of *Ingham et al.* [2008], in an infinite uniform anisotropic medium in which the principal resistivities (ρ_H, ρ_V) are horizontal and vertical the potential at a location (x_j, y_j, z_j) due to a current I injected into the medium from a single electrode at (x_i, y_i, z_i), is given by

$$V = \frac{I\rho_m}{4\pi r_{ij}\left\{1 + (\lambda^2 - 1)\frac{(z_i - z_j)^2}{r_{ij}^2}\right\}^{1/2}}, \tag{1}$$

where ρ_m is the geometric mean resistivity

$$\rho_m = \sqrt{\rho_H \rho_V}, \tag{2}$$

λ is an anisotropy coefficient defined as

$$\lambda = \sqrt{\frac{\rho_V}{\rho_H}} \tag{3}$$

and

$$r_{ij} = \sqrt{(x_i - x_j)^2 + (y_i - y_j)^2 + (z_i - z_j)^2}.$$

Equation (1) may be expressed in the simpler form

$$V = \frac{I\rho_m}{4\pi\left\{X_{ij}^2 + \lambda^2 (z_i - z_j)^2\right\}^{1/2}}, \tag{4}$$

where

$$X_{ij} = \sqrt{(x_i - x_j)^2 + (y_i - y_j)^2} \tag{5}$$

is the horizontal separation between the current and potential electrodes.

[10] The majority of electrical imaging surveys make use of four electrodes. Two electrodes are used to introduce current into the medium, one being a current source the other a sink. The potential difference is then measured between the remaining two electrodes. For a four-electrode system in which current is injected into an anisotropic medium through an electrode C_1 at (x_1, y_1, z_1), is taken out of the medium through an electrode C_2 at (x_2, y_2, z_2), and the potential difference ΔV is measured between electrodes P_1 and P_2 at (x_3, y_3, z_3) and (x_4, y_4, z_4), respectively, equation (1) may be used to show that

$$\Delta V = \frac{I}{4\pi}\rho_m (T_{13} - T_{14} - T_{23} + T_{24}), \tag{6}$$

where

$$T_{ij} = \frac{1}{r_{ij}\left\{1 + (\lambda^2 - 1)\dfrac{(z_i - z_j)^2}{r_{ij}^2}\right\}^{1/2}}.$$

Starting from (6), it is possible to investigate which, if any, combinations of electrodes embedded in an infinite uniform anisotropic medium will allow the direct measurement of individual components of the anisotropic resistivity. This is done by considering the fact that if measurements were made in a medium of uniform isotropic resistivity ρ then the equivalent form of equation (6) would be

$$\Delta V = \frac{I}{4\pi}\rho\left\{\frac{1}{r_{13}} - \frac{1}{r_{14}} - \frac{1}{r_{23}} + \frac{1}{r_{24}}\right\}. \tag{7}$$

Determining the conditions under which (6) reduces to (7) when ρ is considered to be ρ_m, ρ_V or ρ_H, shows which electrode combinations, if any, it is possible to use to yield a determination of the relevant resistivity. Although our interest is primarily in the microstructure of sea ice, for which $\lambda < 1$, the development that follows can easily be adapted for cases where $\lambda > 1$.

2.1. Measurement of ρ_H

[11] The measurement of the horizontal component of the anisotropic resistivity has previously been discussed by *Ingham et al.* [2008]. We summarize those arguments here. As outlined above, measurements can be interpreted in terms of the horizontal component if equation (6), rewritten using (2) and (3) as

$$\Delta V = \frac{I}{4\pi}\rho_H \lambda (T_{13} - T_{14} - T_{23} + T_{24}) \tag{8}$$

is identical to the following form of equation (7)

$$\Delta V = \frac{I}{4\pi}\rho_H\left\{\frac{1}{r_{13}} - \frac{1}{r_{14}} - \frac{1}{r_{23}} + \frac{1}{r_{24}}\right\}. \tag{9}$$

This will be true if in each of the T_{ij} terms in (8)

$$1 + (\lambda^2 - 1)\frac{(z_i - z_j)^2}{r_{ij}^2} = \lambda^2. \tag{10}$$

This is satisfied if

$$(z_i - z_j)^2 = r_{ij}^2,$$

which implies that either

$$(x_i - x_j)^2 + (y_i - y_j)^2 = 0 \tag{11a}$$

or, alternatively, that

$$|z_i - z_j| >> \sqrt{(x_i - x_j)^2 + (y_i - y_j)^2}. \tag{11b}$$

[12] Condition (11b) is met when the current and potential electrodes are much more widely separated vertically than they are horizontally. Although the present discussion concerns an anisotropic medium of infinite extent it is clear that this condition will have practical limitations in a real situation in which the anisotropic structure under study is relatively thin. As this is the case for first year sea ice, for which typical thicknesses are <2 m, we do not consider this possibility.

[13] Condition (11a) corresponds to the current electrode and the potential electrode having the same horizontal location, i.e., being in the same borehole. Applying the same condition to all four T_{ij} terms in equation (8) requires all four electrodes to be in a single borehole. *Timco* [1979] effectively met this condition by using four electrodes aligned vertically in the side of an ice pit to measure ρ_H. However, in the case of four electrodes within the same borehole the formation of an anomalous halo around the electrode string when it is frozen into the ice raises the likelihood that measurements will be significantly affected by ice that is not in its natural state. We therefore exclude this option also.

[14] An additional possibility, as described by *Ingham et al.* [2008], is to consider the situation where C_1 and P_1 have the same horizontal location (i.e., $x_1 = x_3$, $y_1 = y_3$), as do C_2 and P_2 ($x_2 = x_4$, $y_2 = y_4$). In a practical situation this is equivalent to using 2 boreholes, each containing one current and one

potential electrode. This simplifies the expressions for T_{13}, and T_{24} to

$$\lambda T_{ij} = \frac{1}{|z_i - z_j|},$$

while those for T_{14} and T_{23} become

$$\lambda T_{ij} = \frac{\lambda}{\left\{(X_1 - X_2)^2 + (z_i - z_j)^2\right\}^{1/2}\left\{1 + (\lambda^2 - 1)\frac{(z_i - z_j)^2}{(X_1 - X_2)^2 + (z_i - z_j)^2}\right\}^{1/2}},$$

where $X_1 - X_2$ is the horizontal distance between the boreholes.

[15] The expressions for λT_{13} and λT_{24} are clearly equal to the first and last terms on the right hand side of (9). Consider the case that $\lambda < 1$ and the separation of the boreholes is 10 times the smallest vertical electrode separation, i.e.,

$$|z_i - z_j| = n0.1|X_1 - X_2|, \tag{12}$$

where n is an integer. *Ingham et al.* [2008] demonstrate that in these circumstances the dependency on λ in the expressions for λT_{14} and λT_{23} may be approximated as

$$\frac{\lambda}{\left\{1 + (\lambda^2 - 1)\frac{(z_i - z_j)^2}{(X_1 - X_2)^2 + (z_i - z_j)^2}\right\}^{1/2}} \approx \frac{\lambda}{\left\{1 + (\lambda^2 - 1)\frac{0.01n^2}{1 + 0.01n^2}\right\}^{1/2}} \sim \lambda.$$

For $|X_1 - X_2| = 1$, the ratios of the terms in T_{14} and T_{23} to those in T_{13} and T_{24} are then given by

$$(\lambda T_{14}, \lambda T_{23}) : (\lambda T_{13}, \lambda T_{24}) \sim \frac{n\lambda}{10}. \tag{13}$$

If current and potential electrode pairs are chosen such that $n \leq 2$ then, for reasonable values of anisotropy (i.e., λ less than about 0.6, consistent with values reported by *Thyssen et al.* [1974] and *Buckley et al.* [1986]), terms in T_{14} and T_{23} may be ignored compared to those in T_{13} and T_{24}.

[16] It also follows that for $|X_1 - X_2| = 1$, $\lambda < 1$, and values of $n \leq 2$ the terms in (9) in $\frac{1}{r_{14}}$ and $\frac{1}{r_{23}}$ will be significantly less than 1/5 of the size of the terms in $\frac{1}{r_{13}}$ and $\frac{1}{r_{24}}$. Ignoring these smaller terms in equation (9) gives an error of ~10% in the spatial term and within this error equations (8) and (9) may both be approximated by

$$\Delta V = \frac{I}{4\pi}\rho_H\left\{\frac{1}{|z_1 - z_3|} + \frac{1}{|z_2 - z_4|}\right\}. \tag{14}$$

Thus the use of electrodes at two horizontal locations under the conditions that (1) $\lambda < 1$ and (2) the electrodes are positioned such that equation (12) holds, with n small; allows measurements to be made which are sensitive to ρ_H.

2.2. Measurement of ρ_m

[17] To provide a measure of the geometric mean resistivity ρ_m, equation (6) must be equivalent to the expression

$$\Delta V = \frac{I}{4\pi}\rho_m\left\{\frac{1}{r_{13}} - \frac{1}{r_{14}} - \frac{1}{r_{23}} + \frac{1}{r_{24}}\right\}.$$

This requires conditions on the denominators of the expressions for the T_{ij} of the form

$$1 + (\lambda^2 - 1)\frac{(z_i - z_j)^2}{r_{ij}^2} = 1. \tag{15}$$

Equation (15) may be satisfied if

$$z_i = z_j.$$

Extending this so that the conditions are imposed upon all four T_{ij} terms implies that all four electrodes must be at the same vertical level

$$z_1 = z_2 = z_3 = z_4.$$

As it is undesirable to use the same electrode for both current injection and potential measurement, in order to make measurements that will determine ρ_m it is therefore necessary to use a minimum of 4 electrodes at separate horizontal locations (i.e., a minimum of 4 boreholes). In the most general situation where ρ_m is $\rho_m(x, y, z)$, for n boreholes, discounting measurements which simply reverse either the current or potential electrodes, there are therefore $n!/4$ independent measurements that may be made for each vertical level at which there is an electrode.

[18] Measurements of ρ_m may also be obtained by removing either or both of one current and one potential electrode to infinity. For example, under the circumstance of C_2 being at infinity, the expressions for both T_{23} and T_{24} are zero and as long as $z_1 = z_3 = z_4$ then T_{13} and T_{14} are $1/r_{13}$ and $1/r_{14}$, respectively, and both equations (6) and (7) reduce to

$$\Delta V = \frac{I}{4\pi}\rho_m\left\{\frac{1}{r_{13}} - \frac{1}{r_{14}}\right\}.$$

Similarly, if P_2 is at infinity and $z_1 = z_2 = z_3$ (6) and (7) reduce to

$$\Delta V = \frac{I}{4\pi}\rho_m\left\{\frac{1}{r_{13}} - \frac{1}{r_{23}}\right\}.$$

Clearly therefore, using 4 or more electrodes all at separate horizontal locations, there are electrode combinations that may be used to measure the geometric mean resistivity of an infinite uniform anisotropic medium.

2.3. Measurement of ρ_V

[19] To ascertain which, if any, electrode combinations may be used to make measurements which can be used to derive the vertical component of the resistivity ρ_V it is necessary to use equations (2) and (3) to recast equation (6) in the form

$$\Delta V = \frac{I}{4\pi}\frac{\rho_V}{\lambda}(T_{13} - T_{14} - T_{23} + T_{24}).$$

For this equation to take the form which would indicate that measurements are responsive to ρ_V, namely

$$\Delta V = \frac{I}{4\pi}\rho_V\left\{\frac{1}{r_{13}} - \frac{1}{r_{14}} - \frac{1}{r_{23}} + \frac{1}{r_{24}}\right\}$$

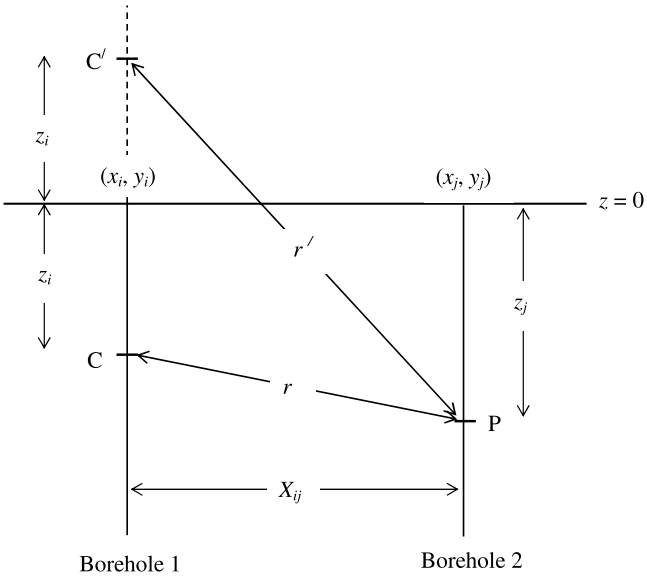

Figure 1. Geometry for the calculation of the potential at electrode P, at (x_j, y_j, z_j), due to current injected at electrode C, at (x_i, y_i, z_i), for the case of a semi-infinite anisotropic medium in the region $z > 0$. The horizontal separation of the electrodes is $X_{ij} = \sqrt{(x_i - x_j)^2 + (y_i - y_j)^2}$.

requires that expressions of the form

$$\frac{1}{1 + (\lambda^2 - 1)\frac{(z_i - z_j)^2}{r_{ij}^2}} = \lambda^2 \tag{16}$$

are satisfied. Equation (16) reduces to

$$\frac{(z_i - z_j)^2}{r_{ij}^2} = -\frac{1}{\lambda^2}, \tag{17}$$

which clearly does not have a real solution. It may therefore be concluded that there are no possible electrode combinations that may be interpreted in terms of the vertical component of the anisotropic resistivity. Having looked at the idealized case of an infinite uniform anisotropic medium, we now turn our attention to a better representation of sea ice, the case of a bounded medium.

3. Cross-Borehole Measurements in a Bounded Anisotropic Medium

[20] In reality cross-borehole resistivity tomography seeks to image the relatively near-surface structure in a half-space of variable resistivity. Although the above theory suggests that measurement of the horizontal component and geometric mean resistivity are possible in an infinite anisotropic medium, this will not necessarily be the case in a bounded anisotropic medium. It is necessary therefore to see how the above results are modified by the inclusion of boundaries.

[21] To consider the effect of boundaries on the potential at a given point in the medium due to a current source elsewhere in the medium we make use of an analogy made in many applied geophysics texts [e.g., *Telford et al.*, 1977] between current flow through a boundary between two media and the optical case of a point light source in one medium separated from another medium by a semitransparent mirror with reflection coefficient k_1. In the optical case the light intensity at a point in the first medium is a combination of the intensity due to the point source and the intensity due to its image in the mirror, diminished by the reflection coefficient. Similarly, the electric potential at a point in the same medium as a point current source can be considered as the sum of the potential due to the source and a generally diminished potential due to an image source. The intensity or potential at a point in the second medium is due only to the point source, but diminished by the transmission coefficient of the boundary.

[22] This situation is illustrated in Figure 1 in which two semi-infinite media are separated by a boundary at $z = 0$ with a reflection coefficient k_1. Current is injected and potential measured in the lower medium which is assumed to be anisotropic. The potential at electrode P at (x_j, z_j) due to current I injected at electrode C at (x_i, z_i) may be expressed, using the form of equations (4) and (5), as

$$V = \frac{I\rho_m}{4\pi\left\{X_{ij}^2 + \lambda^2(z_i - z_j)^2\right\}^{1/2}} + \frac{k_1 I\rho_m}{4\pi\left\{X_{ij}^2 + \lambda^2(z_i + z_j)^2\right\}^{1/2}}. \tag{18}$$

[23] In (18) the first term is the potential due to the actual electrode through which current is injected. The second term is the potential due to the image of C in the boundary. k_1 is the reflection coefficient in the boundary. For current from a source in a medium of resistivity ρ_1, incident on a boundary with a medium of resistivity ρ_2, the reflection coefficient is defined as $k = (\rho_2 - \rho_1)/(\rho_2 + \rho_1)$, thus for the practical case of the upper medium being air ($\rho_2 \sim \infty$), $k_1 = 1$.

[24] The addition of a second boundary at depth t with reflection coefficient k_2 modifies (18) further. In this situation the anisotropic medium is confined to the region $0 \le z \le t$ and multiple images of the current source occur in both boundaries. As given for example by *Keller and Frischknecht* [1966], the potential observed at an electrode (P) in the anisotropic medium at (x_j, y_j, z_j) due to current injected into that medium by an electrode (C) at (x_i, y_i, z_i) is given by

$$\begin{aligned} V_{ij} = \frac{I\rho_m}{4\pi}\Bigg\{ & \frac{1}{\left\{X_{ij}^2 + \lambda^2[z_i - z_j]^2\right\}^{1/2}} \\ & + \sum_{n=1}^{\infty} \frac{k_2^{n-1}}{\left\{X_{ij}^2 + \lambda^2[z_i + z_j + 2(n-1)t]^2\right\}^{1/2}} \\ & + \sum_{n=1}^{\infty} \frac{k_2^{n}}{\left\{X_{ij}^2 + \lambda^2[z_i - z_j - 2nt]^2\right\}^{1/2}} \\ & + \sum_{n=1}^{\infty} \frac{k_2^{n}}{\left\{X_{ij}^2 + \lambda^2[z_i + z_j - 2nt]^2\right\}^{1/2}} \\ & + \sum_{n=1}^{\infty} \frac{k_2^{n}}{\left\{X_{ij}^2 + \lambda^2[z_i - z_j + 2nt]^2\right\}^{1/2}} \Bigg\} \end{aligned} \tag{19}$$

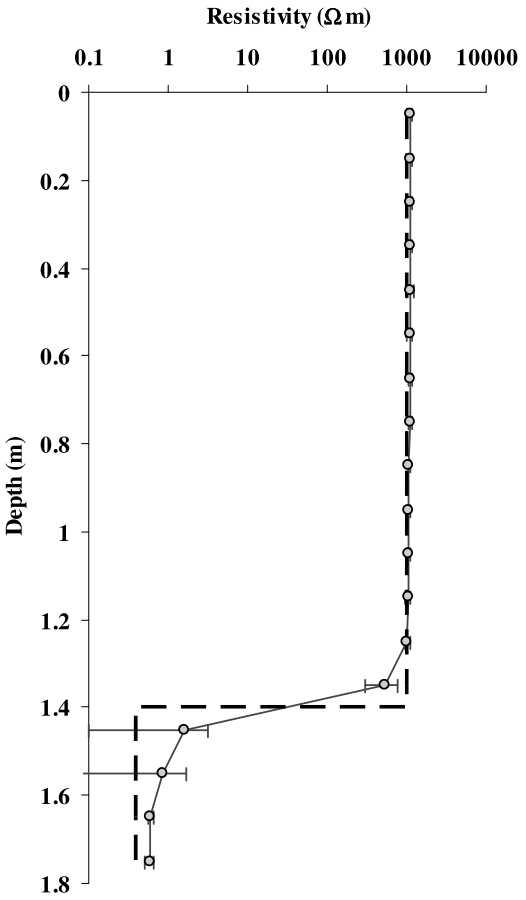

Figure 2. Variation of horizontal resistivity ρ_H with depth recovered by 3-D inversion of synthetic borehole measurements for the case of sea ice of thickness t = 1.4 m, anisotropy coefficient λ = 0.1, and geometric mean resistivity ρ_m = 100 Ωm. The true value of ρ_H is shown by the dashed line.

in which it is been assumed that $k_1 = 1$. Assuming that $\rho_m \approx$ 10–100 Ωm and that the underlying seawater has $\rho_{sw} \approx$ 0.4 Ωm, k_2 will be in the range of −0.92 to −0.99 (the value being negative as ρ_{sw} is less than ρ_m). The first term in (19) represents the potential due to the "direct path" within the anisotropic medium from C to P, whereas the four summations arise from considering the multiple "reflections" from the two boundaries. Similar expressions involving both "direct path" terms and infinite series arising from reflections can be deduced for the other possible combinations of locations of current and potential electrodes: (1) C in the anisotropic medium, P in the underlying half-space; (2) C in the underlying half-space, P in the anisotropic medium; and (3) both C and P in the underlying half-space.

3.1. Measurement of ρ_H

[25] The effect on the measurement of ρ_H of the anisotropic medium being confined to the depth range $0 \le z \le t$, and there being a highly conducting half-space beneath, can be assessed by considering how potential differences calculated from expressions such as (19) compare to those that would exist in an infinite anisotropic medium. As before, the potential difference measured between electrodes in two boreholes separated by horizontal distance X_{ij} is dominated by the potential terms arising from current and potential electrodes that are in the same borehole ($X_{ij} = 0$). As above, we also consider $z_j = z_i + 0.1$ m. Numerical calculation shows that for the relevant likely values of k_2 the four infinite series converge after a few hundred terms. The k_2 dependence in each of the four summations means that whereas the first summation (S_1) is positive, the other three (S_2 to S_4) are negative. For a typical thickness of sea ice of t = 1.4 m, and z_i = 0.1 m (i.e., electrodes close to the upper surface of the ice) $\Sigma S_i = S_1 + S_2 + S_3 + S_4$ is positive and, approximately independently of the value of λ, about 20% of the size of the primary or "direct path" term in (19). The value of ΣS_i decreases with increasing z_i, being ~ 0 at z_i = 0.4 m, and negative and about 66% of the magnitude of the primary potential at z_i = 1.2 m, 0.2 m above the ice-water interface. Thus, even in a bounded anisotropic medium with the typical thickness and parameters relevant to sea ice it appears that estimates of the horizontal component of the resistivity are likely to be within a factor of about 2 of the true value.

[26] To test this a synthetic data set has been generated from the appropriate expressions such as (19)for the case of ρ_m = 100 Ωm and λ = 0.1 (i.e., ρ_H = 1000 Ωm). The synthetic data set comprised over 2000 separate electrode combinations satisfying the restrictions discussed above that allow a measurement of ρ_H to be made. The synthetic data were inverted using the code Res3dinv™ produced by Geotomo Software to derive 3-D models of the horizontal resistivity structure in the volume contained between the boreholes. The code uses a smoothness constrained least squares inversion [*deGroot-Hedlin and Constable*, 1990; *Sasaki*, 1992]. Although the code allows for matrix solution using a quasi-Newton optimization technique [*Loke and Barker*, 1996], all inversions were carried out using a conventional Gauss-Newton method [*Loke and Dahlin*, 2002] which is more appropriate in situations in which large resistivity contrasts, such as between sea ice and underlying seawater, exist. The result of the 3-D inversion of the synthetic data is presented in Figure 2 which shows the mean value of resistivity in each 0.1 m thick layer of the derived 3-D resistivity structure.

[27] It is clear from these results that, given the approximations in the theoretical development, ρ_H is indeed recovered with a good degree of accuracy at all depths within the anisotropic layer between the surface and 1.3 m depth. Only in the layer (1.3–1.4 m), i.e., immediately above the lower interface, is the true horizontal resistivity significantly underestimated. The low resistivity of the underlying seawater (set at 0.4 Ωm for the generation of the synthetic data) is also faithfully recovered. It should be noted that in a real situation the thickness of the anisotropic layer of sea ice is generally known from other measurements. As a result the resistivity below this depth can be constrained to the known resistivity of seawater, as has been applied in the 3-D inversion the result of which shown in Figure 2.

3.2. Measurement of ρ_m

[28] For measurement of ρ_m, using four electrodes at the same level on the corners of a 1 m x 1 m square, the situation is very different. In this case, as X_{ij} = 1 m or $\sqrt{2}$ m, not only is the "direct path" term in (19) significantly smaller, but, for typical thicknesses t ~ 1–2 m, all the S_i are of similar

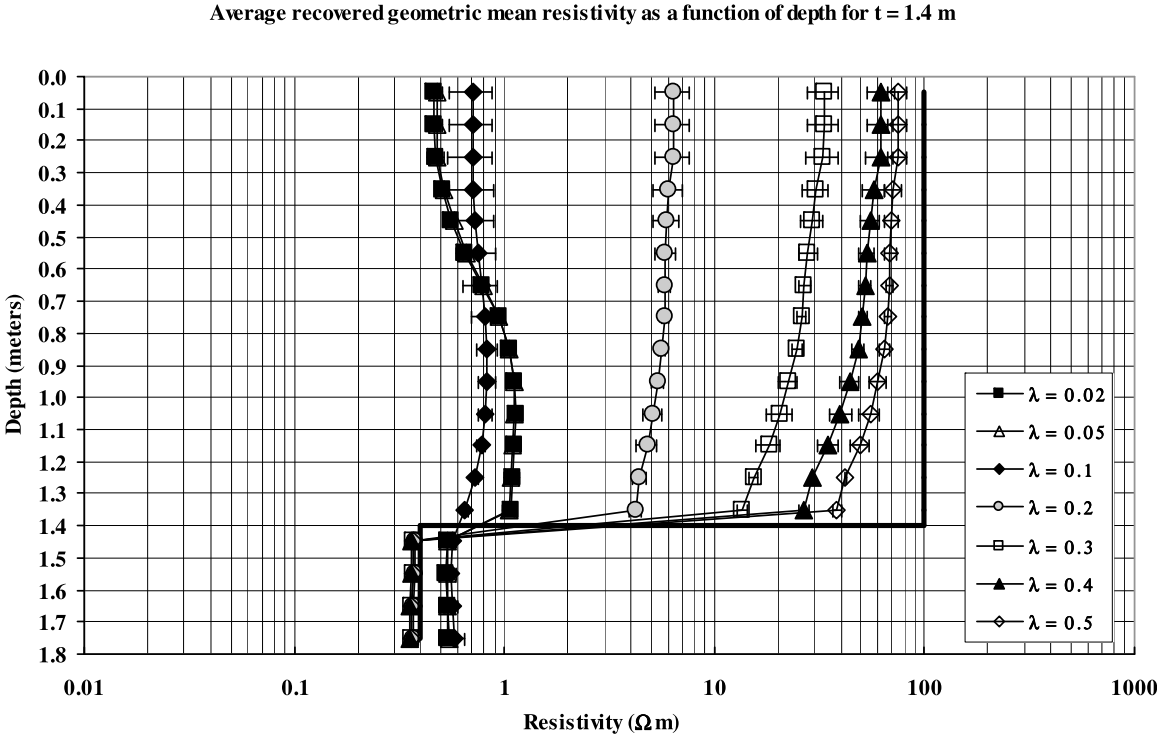

Figure 3. Variation with depth of the value of geometric mean resistivity ρ_m^M recovered by 3-D inversion of synthetic data sets with different values of anisotropy coefficient λ for a true value of the geometric mean resistivity of 100 Ωm and a model ice thickness of 1.4 m shown by the solid line.

magnitude and $\Sigma S_i < 0$. This results not only in the individual potentials due to current being injected or removed from the medium being reduced, but also in the potential difference between P_1 and P_2 being underestimated compared to the case of the infinite anisotropic medium, significantly so for small values of λ. The degree of underestimation depends also on the thickness, t, the depth within the ice of the electrodes being used, and, as k_2 depends upon the resistivity contrast between ρ_m and the underlying seawater, also on the actual value of ρ_m. However, given the likely restricted range of values of k_2 this latter dependence is weak.

[29] The underestimation ρ_m is illustrated in Figure 3 which shows the results of 3-D inversions of synthetic data sets for different values of anisotropy λ for a thickness $t = 1.4$ m and a true value of geometric mean resistivity $\rho_m = 100$ Ωm. The electrode combinations used in generating the synthetic data correspond to those applicable for the measurement of ρ_m in an infinite anisotropic medium. Shown in Figure 3, for different values of λ, are the average values of resistivity in each layer of the derived 3-D resistivity structure. The spatial grid used in the inversion means that in each case these represent an average over 400 cells in each layer. Even for $\lambda = 0.5$, in the upper 1 m of the anisotropic region, the recovered value of ρ_m is only about 70% of the true value. Closer to the ice-water interface the recovered value drops to about 40% of the true value. Similar, but increasingly severe underestimation of ρ_m occurs for decreasing values of λ down to about 0.2. For yet smaller values of λ the recovered value of ρ_m is of the order of only 1% of the true value and has a more complicated variation with depth.

[30] Clearly, once a bounded anisotropic medium of typical thickness is considered, obtaining reliable measurements of geometric mean resistivity of sea ice through DC cross-borehole tomography is not necessarily straightforward. Nevertheless the generation of synthetic data sets from expressions of the form of (19) using the initial criteria for measurement of ρ_m does present a potential resolution of this problem. Inversion of such synthetic data to recover model resistivity values (hereafter referred to as ρ_m^M), makes it possible to derive an empirical parameterization of the relationship between the true value of ρ_m and the recovered value ρ_m^M for different values of t and λ. As t is generally known through independent measurement, and a good estimate of the horizontal component of the resistivity ρ_H can be recovered from cross-borehole measurements, as discussed above, this might allow both ρ_m and λ to be determined as described below.

[31] For example, for a given thickness t of ice the average value of resistivity at some depth, recovered from a 3-D inversion of synthetic data generated for a measurement of ρ_m may be expressed as

$$\rho_m^M = F_z(\lambda)\rho_m, \tag{20}$$

where $F_z(\lambda)$ is a polynomial in the anisotropy coefficient. The form of the polynomial, which describes how the derived value of resistivity, ρ_m^M, is related to the true geometric mean resistivity, ρ_m, can be determined from inversion of synthetic data sets generated for different values

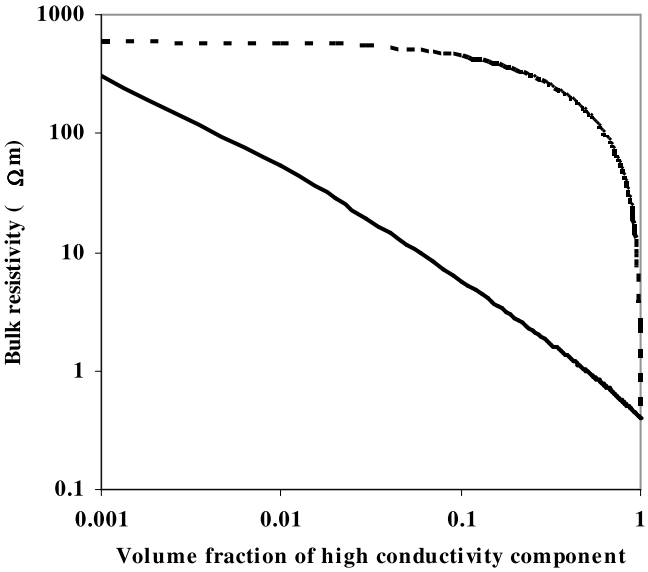

Figure 4. Hashin-Shtrickman bounds on the resistivity of a two-phase mixture in which one component has a resistivity of 0.4 Ωm and the other a resistivity of 600 Ωm. The upper (dashed) curve shows the bulk resistivity as a function of volume fraction of the high-conductivity component when that component occurs as isolated spheres, and the lower (solid) curve shows the bulk resistivity when the high-conductivity component forms a the connected network in which the spheres are embedded.

of λ, such as those shown in Figure 3. Using (2) and (3), equation (20) may be expressed as

$$\rho_m^M = \lambda F_z(\lambda)\rho_H. \quad (21)$$

In principal for any given situation, not only can the form of $F_z(\lambda)$ be deduced from inversion of synthetic data for the particular ice thickness, but ρ_m^M and ρ_H as functions of depth can be determined from inversion of real data. This then allows a value for λ to be found from numerical solution of (21) for each depth range in the resulting 3-D models, and an estimate of the actual value of ρ_m as a function of depth can then be determined from (20).

[32] As an example, in the depth range 0.5–0.6 m in ice of thickness 1.4 m, the results presented in Figure 3 suggest that for $\lambda \leq 0.5$ the function $F_z(\lambda)$ can be represented to a high degree of accuracy by a fourth-order polynomial

$$F_z(\lambda) = -57.411\lambda^4 + 47.077\lambda^3 - 7.1312\lambda^2 + 0.3452\lambda. \quad (22)$$

For the specific case of $\lambda = 0.1$, the inversion of the synthetic data yields a value of ρ_m^M in this depth range of 0.748 Ωm. Additionally, the results in Figure 2 show that the inversion of the separate synthetic data set to determine ρ_H for the case $\rho_m = 100$ Ωm, $\lambda = 0.1$ in this depth range gives a recovered value of ρ_H of 1105 Ωm. Thus (21) allows λ to be found as the numerical solution to

$$0.748 = \left(-57.411\lambda^5 + 47.077\lambda^4 - 7.1312\lambda^3 + 0.3452\lambda^2\right)1105.$$

The result is a value of $\lambda = 0.111$, very close to the true value of 0.1 used in the generation of the synthetic data sets.

[33] Although the above procedure appears, at first sight, to be a resolution of the problem of determining ρ_m, there remain a number of complicating factors when applying this to a real situation. These include (1) the structure of real sea ice may well include a variation in λ with depth which is not incorporated into the synthetic models; (2) in real sea ice the ice-water interface, modeled as a sharp boundary, is not sharply defined; (3) the reliance on the results of 3-D inversions, both of real and synthetic data, may well introduce problems of resolution of resistivity structure; and (4) even in the inversions of synthetic data it is clear, for example from Figure 3, that the derived values of ρ_m^M are relatively insensitive to λ for values of $\lambda \leq 0.1$. Quantifying the uncertainty in derived values of ρ_m resulting from these factors is nontrivial, but as a consequence it is likely that interpretation of values of ρ_m derived in the manner described above should bear in mind that these may only be correct to within a factor of the order of perhaps 3–4.

[34] Given the degree of uncertainty introduced by the above factors it is worth considering the magnitude of resistivity changes that are likely to occur as the internal microstructure of sea ice changes due to expansion and connection of brine pockets and channels within the ice. A simple means of doing this is to consider the Hashin-Shtrikman limits [*Hashin and Shtrikman*, 1962] for the resistivity of a two-phase mixture in which isolated spheres of conductivity σ_2 are surrounded by a connected matrix of conductivity σ_1. The lower and upper limits of bulk resistivity of the mixture (occurring when σ_1 or σ_2, respectively, represents the better conductor) are shown in Figure 4 for the case of a mixture of materials with conductivities (resistivities) of 2.5 S/m (0.4 Ωm) and 0.00167 S/m (600 Ωm). As can be seen, for any volume fraction of high-conductivity component above about 0.5%, the decrease in bulk resistivity between the situations of isolated high-conductivity spheres (i.e., brine pores) and a connected network of high conductivity is 1–3 orders of magnitude. It is clear therefore that, in terms of tracking the changes that occur in the bulk resistivity of sea ice as brine pores expand and connect, the ability to resolve between, for example, bulk resistivities of even 200 and 600 Ωm is not critical. In contrast the ability to distinguish bulk resistivities of 20 and 200 Ωm should enable the development of interconnected brine pore networks to be detected.

4. Field Measurements on First Year Landfast Sea Ice

[35] To demonstrate the application of cross-borehole measurements to recovering the anisotropic resistivity structure in a real situation we present results from a sequence of six separate sets of measurements made on first year landfast sea ice approximately 1 km off the coast of Barrow, Alaska at 71° 21′ 56.45″ N, 156° 32′ 39.01″ W. The measurements were made during the northern hemisphere spring at roughly one to two weekly intervals over the period April–June 2008. A sea ice mass balance site was operated by the University of Alaska Fairbanks at the same location recording snow and ice thickness, sea level, relative humidity and air, ice and water temperatures [*Druckenmiller et al.*, 2009]. The electrode strings used in the resistivity measurements were as described by *Ingham et al.* [2008]

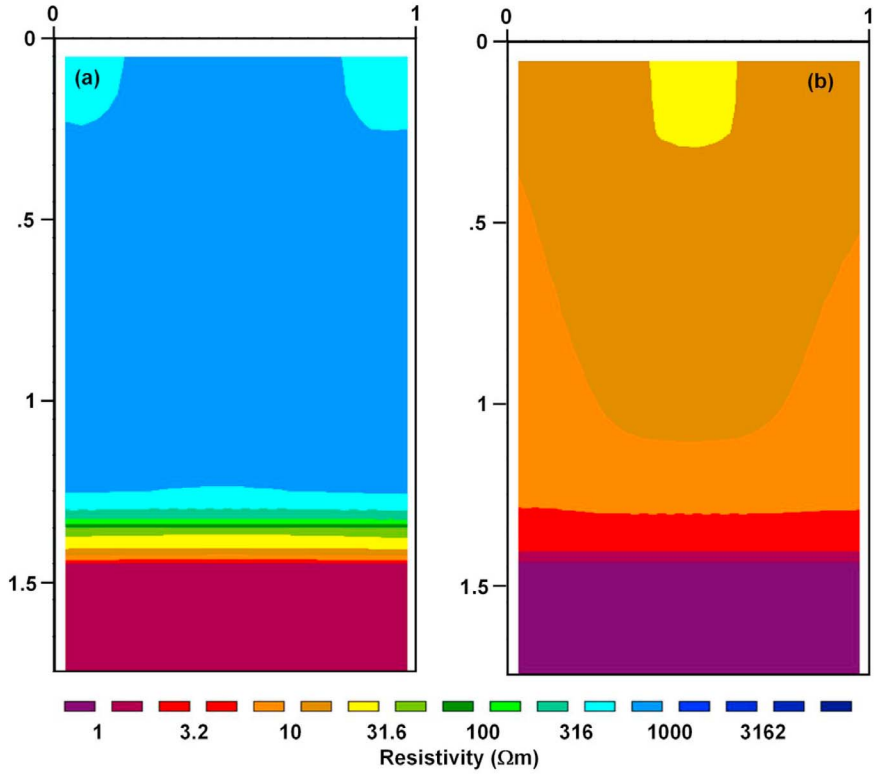

Figure 5. Vertical sections through 3-D structures of (a) ρ_H and (b) ρ_m^M derived by 3-D inversion of field data collected at Barrow over 8 and 9 May 2008. Horizontal distances and depths are both in m.

and were deployed at the corners of a 1 m x 1 m square, allowing measurements to be made through the undisturbed sea ice between boreholes.

[36] On each of the six occasions, measurements of the horizontal resistivity were made between each of the six borehole pairs, with each measurement involving one current and one potential electrode in each borehole, according to the criteria discussed above. Thus, it is assumed that the measurements allow an accurate estimate of ρ_H, in the volume contained by the boreholes, to be derived by 3-D inversion. Similarly, a combination of measurements aimed at determining ρ_m were obtained using a four electrode array with each of the electrodes at approximately the same depth in separate boreholes, and three electrodes at the same depth in separate boreholes and a remote surface electrode. As discussed previously it is assumed that inversion of this data set yields an estimate ρ_m^M of the geometric mean resistivity which is an underestimate of the true value ρ_m.

[37] The data sets for determination of ρ_H contained approximately 2500 separate measurements. Those for ρ_m were smaller and contained between 350 and 400 separate measurements. The ice thickness at the time of each set of measurements was determined from ice temperature measurements and cores. In inversions of the data the thickness values were used to set the initial resistivity below the ice to approximate the resistivity of the underlying seawater (0.4 Ωm). This value was made "sticky" so as to control its degree of change during the inversions. The 3-D inversions for ρ_H typically took 4–6 iterations and gave final RMS misfits of between 10 and 16%, while those for ρ_m took 5–6 iterations and gave final misfits of 2–10%. Much of the misfit in the ρ_H inversions occurs in the region of the ice-water interface. In this region the transition from high resistivity within the ice to the low-resistivity seawater is clearly more complex than for the theoretical models discussed above. As a result it appears that electrodes spaced at vertical intervals of 0.1 m are not able to sample finely enough to accurately resolve the rapid change in resistivity from several hundred Ωm to a value less than 1 Ωm over a vertical distance of typically a few centimeters. The (assumed) much smaller decrease in ρ_m across this same region can, in contrast, be much better reproduced.

[38] Sections through the resulting resistivity structures, obtained from the 3-D inversions of data measured on the 8 and 9 May 2008, showing ρ_H and ρ_m^M are shown in Figures 5a and 5b, respectively. The inversions use a grid with horizontal spacing of 0.05 m in both x and y directions, and a vertical spacing of 0.1 m. Above the immediate vicinity of the ice-water interface, at approximately 1.35 m depth (from ice thickness measurements), ρ_H is seen to be essentially uniform throughout the body of the ice and to have a value around 600 Ωm. Some variation appears in the derived value of ρ_m^M but in general, above the ice-water interface it lies in the range 10–20 Ωm. The vertical discretisation of the model leads to sharp gradients in the recovered values of resistivity between depths of 1.3 and 1.4 m.

[39] As discussed above, synthetic data sets generated for different values of the anisotropy coefficient allow parameterization of the degree to which, for the observed ice thickness, ρ_m^M is an underestimate of the true value of the geometric mean resistivity ρ_m. Synthetic data generated for

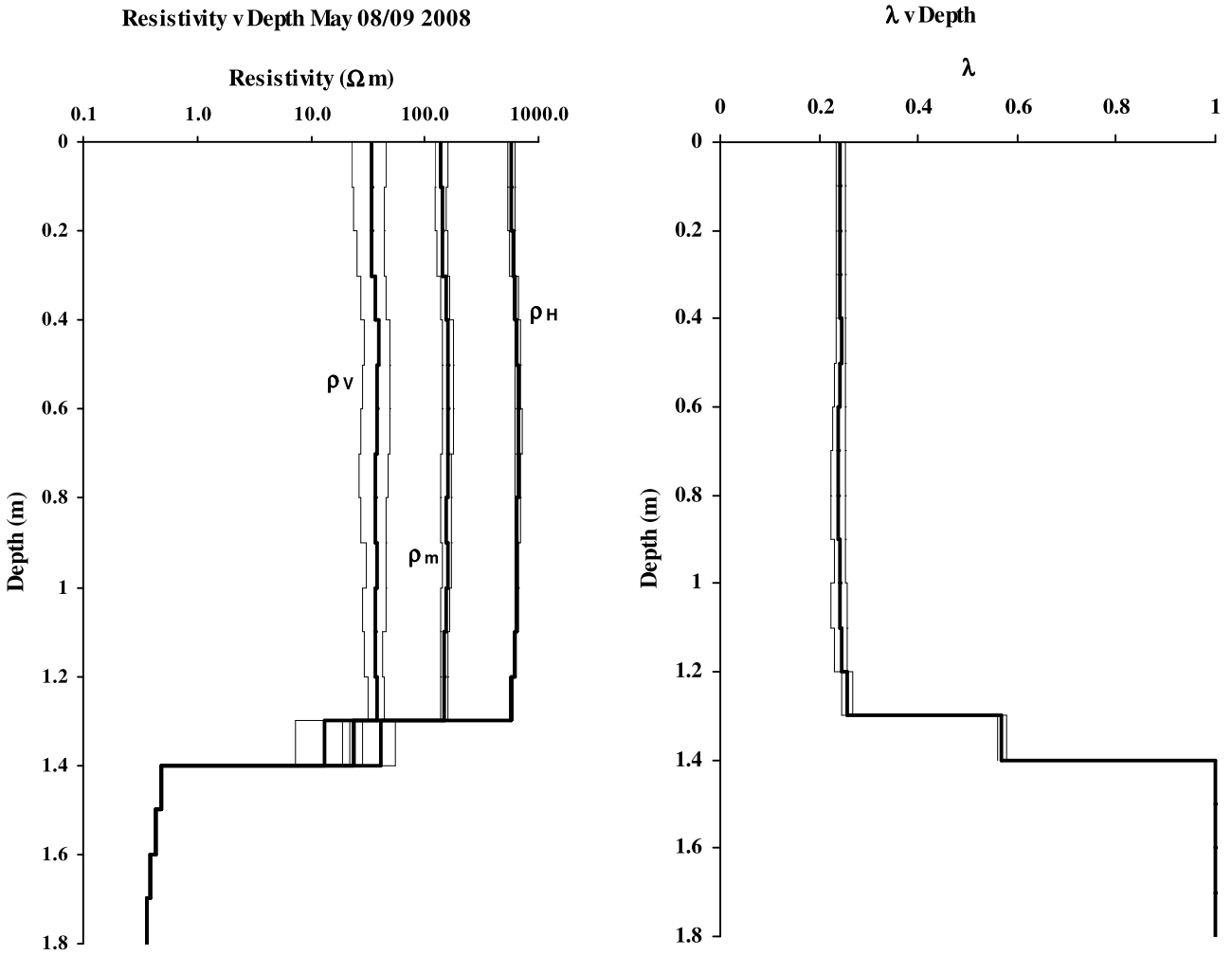

Figure 6. Variations with depth of ρ_H, ρ_m, ρ_V, and λ derived from field data collected at Barrow over 8 and 9 May 2008. Thin lines show limits of the derived values calculated from standard deviations in the average values of ρ_H and ρ_m^M.

different values of anisotropy λ for the measured ice thickness, 1.35 m on 8 and 9 May 2008, have been used to derive the appropriate polynomial $F_z(\lambda)$ for each depth range in the 3-D models. The polynomials have then been used, with the average values of ρ_H and ρ_m^M for each layer in the resistivity models shown in Figure 5, to estimate the actual variation of λ with depth in the ice through numerical solution of (21). These values have then been used with the values of ρ_H to determine not only the true values of ρ_m through the ice, but also to derive the vertical component of the bulk resistivity ρ_V. The standard deviations associated with the average values of ρ_H and ρ_m^M in each layer allow at least a superficial estimate of the uncertainties in λ, ρ_m and ρ_V. The results of this analysis are shown in Figure 6 which shows the derived variation with depth of all three resistivities and the anisotropy coefficient.

[40] For the 8 and 9 May measurements the anisotropy coefficient is found to be close to 0.24 through the entire thickness of the ice down to 1.3 m depth. Although the higher values calculated between 1.3 and 1.4 m are not unreasonable given the expected increase in connectivity of brine at the base of the ice, it must be remembered that this depth range spans the actual ice-water interface and the values of ρ_H and ρ_m^M in this region are not well resolved even though standard deviations calculated from the 3-D models are relatively small. The derived values of λ are slightly less than values found, for example, by *Timco* [1979] at Pond Inlet, N.W.T. (0.59) and *Buckley et al.* [1986] in the Antarctic (~0.5), but are not unreasonable for sea ice formed under the quiescent conditions which tend to exist at Barrow. The corrected values for ρ_m (~ 150 Ωm) are well within the ranges previously measured by other authors using surface resistivity soundings. However, a Wenner array surface sounding taken adjacent to the location of the boreholes on 9 May 2008 yielded apparent resistivity values at small electrode spacing (a = 0.1–0.4 m) of 40–50 Ωm, a factor of about 3 smaller than the values shown in Figure 6. This lends some support to the suggestion that, notwithstanding the small standard deviations in the resolved resistivity values, the cumulative effect of uncertainties and approximations in the derivation of ρ_m may mean that the derived values should be regarded as an estimate correct to within a factor of 3–4. However, various authors have previously noted the nonuniqueness in the interpretation of

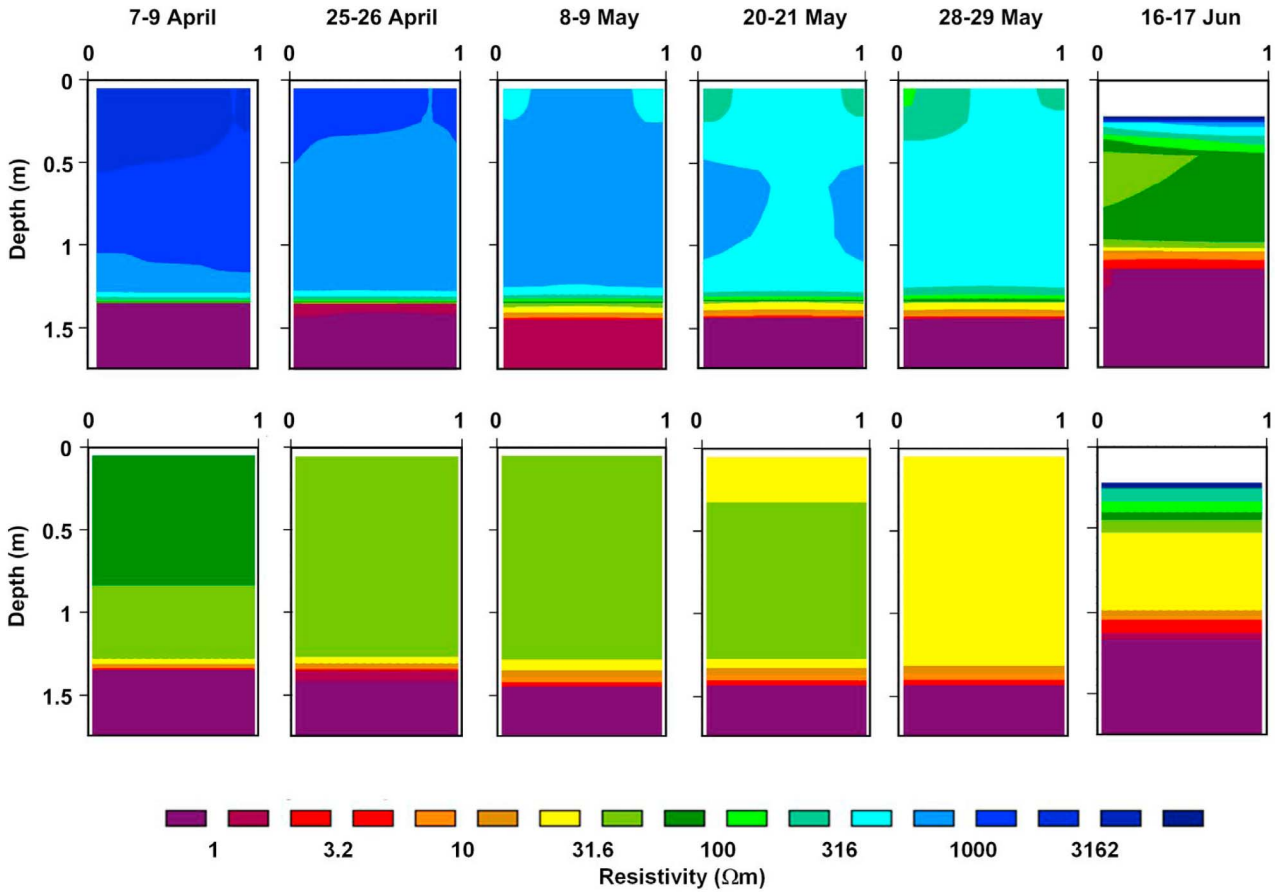

Figure 7. Vertical sections through derived ρ_H and calculated ρ_V structures for a sequence of six dates between April and June 2008. (top) The ρ_H and (bottom) ρ_V are shown. Horizontal distances and depths are both in m.

Wenner soundings, particularly the distortions in derived depth variations that occur in interpretation due to the anisotropic nature of the resistivity. It could therefore be argued that the estimates of ρ_m derived from the cross-borehole results are in fact more reliable. In the context of mapping how the resistivity structure of sea ice varies with time over a series of measurement sequences such an unresolved ambiguity may not necessarily be crucial.

[41] Each of the data sets in the entire sequence of measurements from April–June 2008 was treated in the manner described above to derive both the horizontal and vertical components of resistivity. Vertical sections through the derived models for ρ_H and the calculated profiles for ρ_V, for all six sets of measurements are shown in Figure 7. From these results it is clear that, as originally found by *Ingham et al.* [2008] for ρ_H, there are significant temporal changes in resistivity as spring warming occurs. These may be summarized as follows:

[42] 1. There is a gradual decrease of ρ_H from over 1000 Ωm to about 350 Ωm between early April and the end of May.

[43] 2. A similar, but smaller, change in the vertical component of resistivity ρ_V occurs over the same period. Values decrease from 40–70 Ωm in early April to less than 30 Ωm by the end of May.

[44] 3. Despite these changes the anisotropy coefficient λ remains approximately constant with values (0.2–0.3) similar to those shown in Figure 6.

[45] 4. A more significant change in the horizontal component of resistivity take place between the end of May and mid-June during which the resistivity decreases by a factor of about 6. During this period there was a considerable thinning of the ice as well as surface ablation which left the upper three electrodes in each string no longer embedded in the ice.

[46] 5. Over this period in early June there was also a decrease in the vertical resistivity between 0.5 and 1 m depth, while at shallower depths the infiltration of fresh water, from melt ponds formed on the surface, led to an increase in ρ_V.

5. Discussion

[47] Many authors have discussed pronounced changes in the physical properties of sea ice with time and temperature. For example, *Buckley and Trodahl* [1987] commented on changes in the optical behavior of Antarctic sea ice related to a 10°C increase in temperature. *Pringle et al.* [2007], in studying the thermal conductivity of sea ice, estimated that periodic internal motion of brine within the ice due to convection could contribute to the total heat flow through

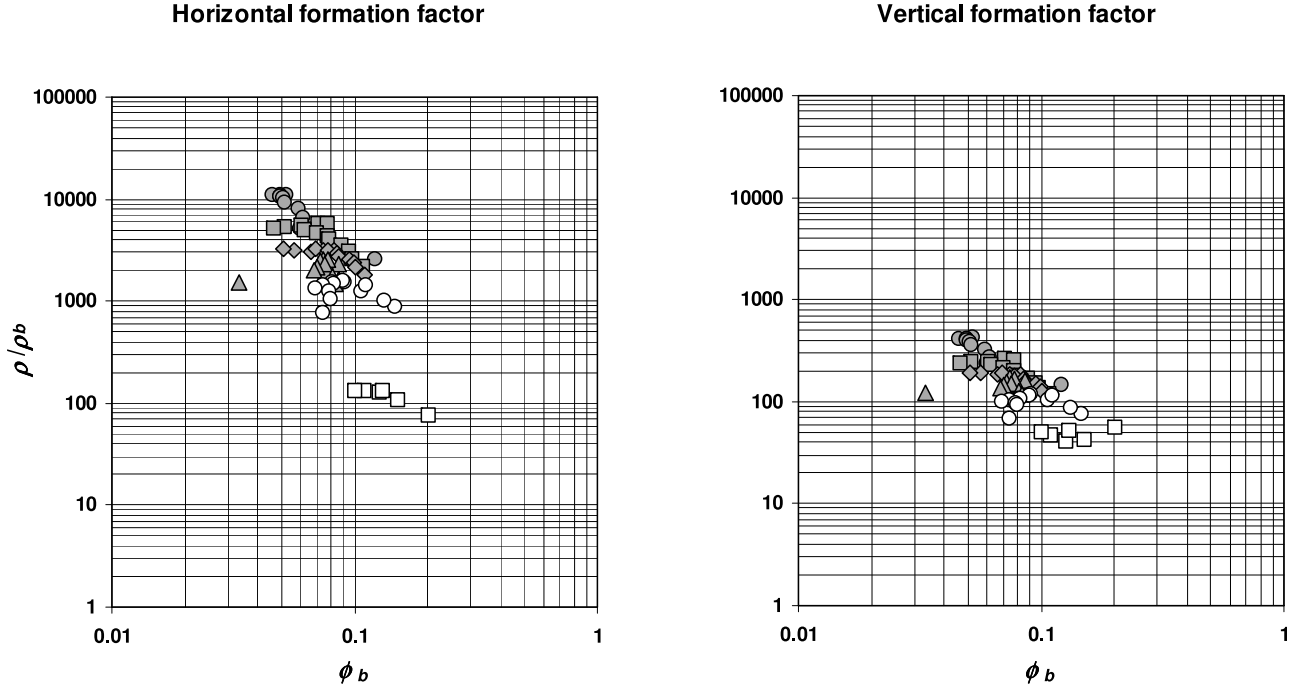

Figure 8. Plots of formation factor (ρ/ρ_b) against brine volume fraction (ϕ_b) for horizontal and vertical components of resistivity. Solid circles are data from 7 to 9 April, solid squares are data from 25 to 26 April, solid diamonds are data from 8 to 9 May, solid triangles are data from 20 to 21 May, open circles are data from 28 to 29 May, and open squares are data from 16 to 17 June.

the ice. *Golden et al.* [2006] have also emphasized the importance of the fluid permeability of sea ice for not only understanding brine drainage and the growth of ice, but also the transport of nutrients and pollutants through sea ice. In particular, below −5°C sea ice appears to be vertically impermeable [*Weeks and Ackley*, 1986], whereas above this temperature it is permeable [*Golden et al.*, 2007].

[48] The results shown in Figure 7 are possibly the first presentation of the temporal evolution of an anisotropic physical property of sea ice. They make it clear that the electrical properties of sea ice undergo significant changes. Detailed modeling of ice structure to attempt to fully understand how these changes relate to temperature, salinity and brine volume fraction (ϕ_b) remains to be carried out. Nevertheless it is likely, as is discussed further below, that the decrease in both principal components of resistivity between early April and late May is related to an increase in ϕ_b as the ice warms. However, the relatively low values of vertical resistivity which exist even when the ice is still cold in early April, suggests that, although the ice may be impermeable to fluid transport, a certain degree of electrical connectivity exists at all times. Given the apparent existence of vertical electrical connection, the implications for fluid permeability of the structural changes which lead to the changes in electrical resistivity warrant considerable attention.

[49] Some initial indication of the nature of the variation of resistivity with brine volume fraction can be gained by calculating the manner in which the formation factor, *FF*, (defined as the ratio of the bulk resistivity ρ of a saturated medium to the resistivity of its pore fluid, ρ_b) varies with ϕ_b. The concept of formation factor derives from Archie's law [*Archie*, 1942] which relates these parameters through the expression

$$FF = \frac{\rho}{\rho_b} = C\phi_b^{-m} \tag{23}$$

in which C and m are empirically determined constants. The first of these constants, C, is a function of the microstructure of the medium and, as long as the geometry of this remains unchanged a log-log plot of formation factor against brine volume fraction yields a straight line of slope $-m$. For the resistivity models shown in Figure 7, the corresponding values of brine resistivity can be calculated from the measured temperature data using the relationship of *Morey et al.* [1984], and brine volume fractions can be found from measured temperature and salinity data using the expressions of *Cox and Weeks* [1983]. The resulting log-log plots of *FF* against ϕ_b for both the horizontal and vertical components of the bulk resistivity are shown in Figure 8 and, for brine volume fractions less than 10%, clearly confirm the expected linear variation. In addition to this, however, the sharp drop in the horizontal component of resistivity between late May and mid-June, which is prominent in Fig, 7, appears as a sharp discontinuity in the formation factor plot. This is possibly indicative of a fundamental change in the microstructure of the ice and suggests that a percolation threshold such as proposed by *Golden et al.* [1998, 2007] may have been crossed. *Ingham et al.* [2008] tentatively suggested that such a threshold might occur for the horizontal component of resistivity at a brine volume fraction of about 8%. That estimate was based, however, on three sets of much sparser data acquired using only 2 boreholes.

Detailed analysis and structural modeling of the present results should give a much clearer indication of any such threshold and also provide information on the existence of any percolation transition for the vertical component of resistivity.

[50] The vertical conductivity structure, in particular the near-constant values of the anisotropy coefficient λ shown in Figure 6, also suggests that vertical microstructural variations associated with the transition from granular to columnar ice (which was observed to occur at depths between 20 and 40 cm in the vicinity of the measurement site) are not strongly reflected in the resistivity structure. While this finding requires more detailed analysis and measurements at finer vertical resolution, it may suggest that in granular ice, rather than the isotropic primary pore space, it is the anisotropic secondary pores (such as brine tubes and channels) that control the resistivity structure. Similarly, the impact of vertical variations in brine volume fractions is only marginally expressed in the structure of ρ_H and ρ_V (Figure 6).

6. Summary

[51] We have shown theoretically that suitable combinations of cross-borehole DC resistivity measurements may be used to measure directly the value of the horizontal component of the resistivity in sea ice or other anisotropic medium within which $\rho_V < \rho_H$. Furthermore, although the particular structure of sea ice means that exact measurement of the geometric mean resistivity is not possible, we have demonstrated that it is also possible to make measurements which, in association with numerical modeling, allow a reasonable estimate of ρ_m to be derived. As a consequence estimates of the vertical component of resistivity, which cannot be directly measured, can also be obtained. The technique is illustrated by the results of a series of measurements made on first year sea ice at Barrow, Alaska. These clearly show that the electrical resistivity of sea ice varies significantly with time and temperature. The development described here thus opens the way for understanding the microstructural changes that occur within sea ice and the implications of these for the behavior of other transport properties. It therefore has the potential to contribute significantly to the understanding of sea ice microstructure and its response to changes in temperature, salinity and ϕ_b.

[52] **Acknowledgments.** K.J. is supported by a Victoria University of Wellington Postgraduate Assistantship. We acknowledge financial support through NSF Office of Polar Programs grants ARC-0620124 and 0934683 and logistic support provided by the Barrow Arctic Science Consortium. The authors wish to thank Hugh Bibby and two anonymous reviewers for comments on an earlier version of the manuscript.

References

Archie, G. E. (1942), The electrical resistivity log as an aid in determining some reservoir characteristics, *Trans. Am. Inst. Min. Metall. Pet. Eng.*, *146*, 54–62.

Bhattacharya, P. K., and H. P. Patra (1968), *Direct current Geoelectric Sounding: Principles and Interpretation*, 139 pp., Elsevier, Amsterdam.

Buckley, R. G., and H. J. Trodahl (1987), Thermally driven changes in the optical properties of sea ice, *Cold Reg. Sci. Technol.*, *14*, 201–204, doi:10.1016/0165-232X(87)90036-X.

Buckley, R. G., M. P. Staines, and W. H. Robinson (1986), In situ measurements of the resistivity of Antarctic sea ice, *Cold Reg. Sci. Technol.*, *12*, 285–290, doi:10.1016/0165-232X(86)90041-8.

Callaghan, P. T., C. D. Eccles, T. G. Haskell, P. J. Langhorne, and J. D. Seymour (1998), Earth's field NMR in Antarctica: A pulsed gradient spin echo NMR study of restricted diffusion in sea ice, *J. Magn. Reson.*, *133*, 148–154, doi:10.1006/jmre.1998.1417.

Callaghan, P. T., R. Dykstra, C. D. Eccles, T. G. Haskell, and J. D. Seymour (1999), A nuclear magnetic resonance study of Antarctic sea ice brine diffusivity, *Cold Reg. Sci. Technol.*, *29*, 153–171, doi:10.1016/S0165-232X(99)00024-5.

Cherkaeva, E., and K. M. Golden (1998), Inverse bounds for microstructural parameters of composite media derived from complex permittivity measurements, *Waves Random Complex Media*, *8*, 437–450, doi:10.1088/0959-7174/8/4/004.

Comiso, J. C. (2003), Large-scale characteristics and variability of the global sea ice cover, in *Sea Ice: An Introduction to its Physics, Chemistry, Biology and Geology*, edited by D. N. Thomas and G. S. Dieckmann, pp. 112–142, Blackwell Sci., Oxford, U. K.

Cox, G. F. N., and W. F. Weeks (1983), Equations for determining the gas and brine volumes in sea-ice samples, *J. Glaciol.*, *29*, 306–316.

deGroot-Hedlin, C., and S. Constable (1990), Occam's inversion to generate smooth two-dimensional models from magnetotelluric data, *Geophysics*, *55*, 1613–1624, doi:10.1190/1.1442813.

Dieckmann, G. S., and H. H. Hellmer (2003), The importance of sea ice: An overview, in *Sea Ice: An Introduction to its Physics, Chemistry, Biology and Geology*, edited by D. N. Thomas and G. S. Dieckmann, pp. 1–21, Blackwell Sci., Oxford, U. K.

Druckenmiller, M. L., H. Eicken, M. A. Johnson, D. J. Pringle, and C. C. Williams (2009), Towards an integrated coastal sea-ice observatory: System components and a case study at Barrow, Alaska, *Cold Reg. Sci. Technol.*, *56*, 61–72, doi:10.1016/j.coldregions.2008.12.003.

Eicken, H. (2003), From the microscopic, to the macroscopic, to the regional scale: Growth, microstructure and properties of sea ice, in *Sea Ice: An Introduction to its Physics, Chemistry, Biology and Geology*, edited by D. N. Thomas and G. S. Dieckmann, pp. 22–81, Blackwell Sci., Oxford, U. K.

Eicken, H., C. Bock, R. Wittig, H. Miller, and H.-O. Poertner (2000), Magnetic resonance imaging of sea ice pore fluids: Methods and thermal evolution of pore microstructure, *Cold Reg. Sci. Technol.*, *31*, 207–225, doi:10.1016/S0165-232X(00)00016-1.

Freitag, J., and H. Eicken (2003), Melt water circulation and permeability of Arctic summer sea ice derived from hydrological field experiments, *J. Glaciol.*, *49*, 349–358, doi:10.3189/172756503781830601.

Fritsen, C. H., V. I. Lytle, S. F. Ackley, and C. W. Sullivan (1994), Autumn bloom of Antarctic pack-ice algae, *Science*, *266*, 782–784, doi:10.1126/science.266.5186.782.

Fujino, K., and Y. Suzuki (1963), An attempt to estimate the thickness of sea ice by electrical resistivity method II, *Low Temp. Sci. Ser. A*, *21*, 151–157.

Golden, K. M., S. F. Ackley, and V. I. Lytle (1998), The percolation phase transition in sea ice, *Science*, *282*, 2238–2241, doi:10.1126/science.282.5397.2238.

Golden, K. M., A. L. Heaton, H. Eicken, and V. I. Lytle (2006), Void bounds for fluid transport in sea ice, *Mech. Mater.*, *38*, 801–817, doi:10.1016/j.mechmat.2005.06.015.

Golden, K. M., H. Eicken, A. L. Heaton, J. Miner, D. J. Pringle, and J. Zhu (2007), Thermal evolution of permeability and microstructure in sea ice, *Geophys. Res. Lett.*, *34*, L16501, doi:10.1029/2007GL030447.

Hallikainen, M., and D. P. Winebrenner (1992), The physical basis for sea ice remote sensing, in *Microwave Remote Sensing of Sea Ice*, *Geophys. Monogr. Ser.*, vol. 68, edited by F. D. Carsey, pp. 29–46, AGU, Washington, D. C.

Hashin, Z., and S. Shtrikman (1962), A variational approach to the theory of the effective magnetic permeability of multiphase materials, *J. Appl. Phys.*, *33*, 3125–3131, doi:10.1063/1.1728579.

Ingham, M., D. Pringle, and H. Eicken (2008), Cross-borehole resistivity tomography of sea ice, *Cold Reg. Sci. Technol.*, *52*, 263–277, doi:10.1016/j.coldregions.2007.05.002.

Kawamura, T. (1988), Observations of the internal structure of sea ice by x ray computed tomography, *J. Geophys. Res.*, *93*, 2343–2350, doi:10.1029/JC093iC03p02343.

Keller, G. V., and F. C. Frischknecht (1966), *International Series of Monographs in Electromagnetic Waves*, vol. 10, *Electrical Methods in Geophysical Prospecting*, Pergamon, Oxford, U. K.

Kovacs, A., and R. Morey (1978), Radar anisotropy of sea ice due to preferred azimuthal orientation of the horizontal c axes of ice crystals, *J. Geophys. Res.*, *83*, 6037–6046, doi:10.1029/JC083iC12p06037.

Krembs, C., R. Gradinger, and M. Spindler (2000), Implications of brine channel geometry and surface area for the interaction of sympagic organisms in Arctic Sea ice, *J. Exp. Mar. Biol. Ecol.*, *243*, 55–80, doi:10.1016/S0022-0981(99)00111-2.

Loke, M. H., and R. D. Barker (1996), Rapid least-squares inversion of apparent resistivity pseudosections by a quasi-Newton method, *Geophys. Prospect.*, *44*, 131–152, doi:10.1111/j.1365-2478.1996.tb00142.x.

Loke, M. H., and T. Dahlin (2002), A comparison of the Gauss-Newton and quasi-Newton methods in resistivity imaging inversions, *J. Appl. Geophys.*, *49*, 149–162, doi:10.1016/S0926-9851(01)00106-9.

Mercier, O. R., M. W. Hunter, and P. T. Callaghan (2005), Brine diffusion in first-year sea ice measured by Earth's field PGSE-NMR, *Cold Reg. Sci. Technol.*, *42*, 96–105, doi:10.1016/j.coldregions.2004.12.004.

Morey, R. M., A. Kovacs, and G. F. N. Cox (1984), Electromagnetic properties of sea ice, *Cold Reg. Sci. Technol.*, *9*, 53–75, doi:10.1016/0165-232X(84)90048-X.

Notz, D., and M. G. Worster (2008), In situ measurements of the evolution of young sea ice, *J. Geophys. Res.*, *113*, C03001, doi:10.1029/2007JC004333.

Perovich, D. K. (1998), Optical properties of sea ice, in *Physics of Ice-Covered Seas*, edited by M. Lepparanta, pp. 195–230, Springer, New York.

Pringle, D. J., H. Eicken, H. J. Trodahl, and L. G. E. Backstrom (2007), Thermal conductivity of landfast Antarctic and Arctic sea ice, *J. Geophys. Res.*, *112*, C04017, doi:10.1029/2006JC003641.

Pringle, D. J., G. Dubuis, and H. Eicken (2009a), Impedance measurements of the complex dielectric permittivity of sea ice at 50 MHz: Pore microstructure and potential for salinity monitoring, *J. Glaciol.*, *55*, 81–94, doi:10.3189/002214309788608903.

Pringle, D. J., J. E. Miner, H. Eicken, and K. M. Golden (2009b), Pore-space percolation in sea ice single crystals, *J. Geophys. Res.*, *114*, C12017, doi:10.1029/2008JC005145.

Sasaki, Y. (1992), Resolution of resistivity tomography inferred from numerical simulation, *Geophys. Prospect.*, *40*, 453–463, doi:10.1111/j.1365-2478.1992.tb00536.x.

Telford, W. M., L. P. Geldart, R. E. Sheriff, and D. A. Keys (1977), *Applied Geophysics*, Cambridge Univ. Press, New York.

Thyssen, F., H. Kohnen, M. V. Cowan, and G. W. Timco (1974), DC resistivity measurements on sea ice near Pond Inlet, N.W.T (Baffin Island), *Polarforschung*, *44*, 117–126.

Timco, G. W. (1979), An analysis of the in-situ resistivity of sea ice in terms of its microstructure, *J. Glaciol.*, *22*, 461–471.

Tinga, W. R., W. A. G. Voss, and D. F. Blossey (1973), Generalized approach to multiphase dielectric mixture theory, *J. Appl. Phys.*, *44*, 3897–3902, doi:10.1063/1.1662868.

Weeks, W. F. (1998), Growth conditions and the structure and properties of sea ice, in *Physics of Ice-Covered Seas*, edited by M. Lepparanta, pp. 25–104, Springer, New York.

Weeks, W. F., and S. F. Ackley (1986), The growth, structure and properties of sea ice, in *The Geophysics of Sea Ice*, edited by N. Untersteiner, pp. 9–164, Plenum, New York.

H. Eicken and D. J. Pringle, Geophysical Institute, University of Alaska Fairbanks, 903 Koyukuk Dr., Fairbanks, AK 99775-7320, USA.

M. Ingham and K. A. Jones, School of Chemical and Physical Sciences, Victoria University of Wellington, PO Box 600, Wellington 6140, New Zealand. (malcolm.ingham@vuw.ac.nz)